A Full Wave Simulation of Disturbances in Picosecond Signals by Electro-Optic Probing

David Conn, Xiaohua Wu, Jian Song and Kent Nickerson

Communications Research Laboratory
McMaster University
Hamilton, Ontario, Canada L8S 4K1

Abstract

Disturbances induced in electric fields near coplanar waveguides by electro-optic dielectric sampling probes are studied using a three dimensional FD-TD technique. Probing effects on the waveguide S-parameters are characterized and the signal field distortion in the optical tip is calculated. It is found that probes can have a significant effect on measurement accuracy in the subpicosecond domain, and that optical samples taken near the edge of the probe can result in measurements with less distortion than those taken at the center.

1 Introduction

Electro-optic (E-O) sampling is a promising measurement technique for high-speed opto-electronic devices and circuits [1]. External E-O sampling, which incorporates a birefringent dielectric probe immersed in the electric field to be measured, affords great measurement versatility. The sampling system sensitivity increases with the degree of field immersion, but so do probe effects. Though E-O measurement is becoming more practical and popular, calibration for probe effects has received little attention. Consequently, most E-O sampling measurements have been done in relative terms [1]-[3].

In this paper, we present a new field modelling technique for evaluating the fundamental performance limits of external E-O sampling systems. The disturbances induced on a subpicosecond impulse signal field by a probe are modelled, and the associated scattering parameters of the measured coplanar waveguide(CPW) are calculated. We find that the signal field distortion, as observed in the optical tip, results in significant discrepancies from ideal measurements of subpicosecond pulses. Our method allows optimal choices for probe positioning and the optical sampling point. Based on detailed modelling, a field-based calibration technique can be developed to compensate for field disturbances in external E-O sampling. This technique is essential to quantitatively characterize devices and to extend E-O system performance to the subpicosecond domain. Hence, we present a universal method of calibrating E-O measurement systems that can be applied to a broad class of experimental configurations.

2 Field disturbances in E-O sampling

Fig. 1 shows an external E-O measurement configuration for obtaining CPW electric fields. Because of the close placement of an optical probe's tip, which has a dielectric constant as large as $\epsilon_r = 43$, the assumption of negligible disturbance to the sampled field and to the device under test is questionable. Hence, modelling field disturbances is required to derive quantitative measurements. A two-dimensional static field model of an E-O probe has been used to analyze the sensitivity of the measurement system [4]. Unlike the method used in [4], the finite-difference time-domain (FD-TD) [5] method enables us to deal with high speed signals, dispersive effects and three dimensional probing discontinuities.

3 Field modelling of the optical probe

3.1 Description of the problem

The E-O probe simulation, as depicted in Fig. 1, is based on the Terametrics Model 200. The birefringent material is a $200\mu m$ by $200\mu m$ square of $20\mu m$ thick lithium tantalate ($LiTaO_3$) supported by a truncated pyramid of silica. The pyramid is approximated in simulation by a stacked staircase of square layers. The tip face is centred on and parallel to the CPW traces. The FD-TD technique is used in three dimensional field modelling. A $0.6ps$ full-wave-at-half-maxima (FWHM) Gaussian pulse [2] is launched in the z-direction towards the probe. The parameters of the simulation are listed in Table-1.

We define the electric field vector: $\vec{\mathbf{E}} = E_x\hat{\mathbf{x}} + E_y\hat{\mathbf{y}} + E_z\hat{\mathbf{z}}$.

Three cases are considered in the simulation: Probe face $10\mu m$ above the CPW (Case 1); probe contacting the CPW (Case 2); and no probe (Case 3). For each of these cases, disturbances to the CPW are characterized in terms of S-parameters. The difference between the measured and the actual CPW signal field is defined as the signal field distortion.

3.2 Results and discussion

Field distributions

Fig. 2 shows the distribution of E_y $10\mu m$ above the CPW

Distance(CPW to tip) **Case 1** h_1 (μm)	10.0
Distance(CPW to tip) **Case 2** h_1 (μm)	0.0
Distance(CPW to tip) **Case 3** h_1 (μm)	∞
Center strip width s (μm)	1.0
Slot spacing width w (μm)	10.0
Optical tip width w_1 (μm)	200.0
Optical tip thickness h_2 (μm)	20.0
Substrate thickness h (μm)	500.0
Substrate dielectric constant ϵ_{r1}	13.2
Optical tip dielectric constant ϵ_{r2}	43.0
Probe supporter dielectric constant ϵ_{r3}	4.5
Space step dx (μm)	10.0
Space step dy (μm)	5.0
Space step dz (μm)	6.0
Time step dt (ps)	0.01
Mesh number in x-direction n_1	92
Mesh number in y-direction n_2	20
Mesh number in z-direction n_3	188

Table-1: Parameters in FD-TD analysis

in Cases 1 and 3 at the time when the pulse peak reaches the probe center point **C** in Fig. 1. The field disturbances, as seen in Fig. 2, are attributed to the discontinuity and surface waves introduced by the probe. Two peaks in Fig. 2(b) occur exactly at the edges of the probe.

Fig. 3 gives E_z waveforms in Cases 1 and 3 at point **C**. While E_z is negligible with no probe (Case 3), it is greatly changed in the presence of the probe. This indicates that the quasi-TEM mode of propagation in the CPW is significantly affected.

Disturbances to the CPW

The magnitude of the reflection coefficient S_{11} of the CPW for Cases 1 and 2 is shown in Fig. 4. At 50GHz, the reflection is less than $-40dB$ in Case 1, but increases to $-7dB$ in Case 2. Fig. 5 gives the transmission coefficient S_{21} of the CPW for Cases 1,2 and 3. Cases 1 and 3 have almost the same S_{21}. Case 2, however, shows a decrease in magnitude of about $-1.5dB$ at 50GHz and a phase change of 30 degrees. Radiation loss and surface waves make the sum of S_{11} and S_{21} less than unity.

Fig. 6 shows the superposed pulse signal fields for the three cases. While the delay, relative to the unprobed case, is negligible in Case 1, about $1.8ps$ of delay appears in Case 2, which corresponds to the 30 degree phase shift in the frequency domain.

These results indicate that the assumption of negligible disturbance to the device under test is acceptable only if the probe is reasonably far away from the device. From our simulation, one could assume good measurement results for a probe tip spacing of $10\mu m$ or more.

Signal field distortion in the optic tip

Fig. 7 displays the E_y component at the probed points **A,B** and **C** shown in Fig. 1. Case 3 (Fig. 7(a)), indicates little distortion, but Case 1 (Fig. 7(b)) shows a significant effect of probing. First, the rise time of the pulse increases while the fall time decreases slightly, explaining discrepancies between the measured and the simulated results in [2]. Secondly, the pulse-width narrows in the tip. Finally, a large negative tail and ringing are predicted.

These features imply that sampled signal fields can be nonlinear to the response in the CPW. In fact, the optical tip acts as a dielectric resonant device. For the given dimensions, the tip resonant frequency is approximately 600GHz.

It is shown that the sampled signal field in the optical tip can be significantly different from the unprobed field. Hence, a field-based calibration technique should be developed to take this difference into account.

Optimal sampling point in the optical tip

As shown in Fig. 7, signal field distortion can be quantified as a function of the position where the field is sampled. The physical center of the tip is usually considered as the ideal position to sample a field [4]. However, our results suggest that optical sampling near the leading edge of the probe tip can lead to less waveform distortion. Figures 8(a) and 8(b) compares E_y in the optical tip at respective points **C** and **D**(See Fig. 1), the latter is only $13\mu m$ away from the edge. The reduced distortion at the edge is attributed to the frequency dependent response of the tip to the field pulse.

4 Conclusions

Field disturbances induced on a CPW by an E-O sampling probe have been simulated in three dimensions, and the corresponding changes in the waveguide S-parameters calculated for a set of probe face to CPW distances. Signal field distortion in the optical tip has been observed and signal field fidelity as measured by E-O sampling at points in the optical tip studied. Results indicate that sampling near the leading edge of the probe tip can result in less distortion than sampling at the probe's center. Based on our field modelling, a field-based calibration technique will be attempted to compensate effects of disturbances in E-O sampling. This is essential for the extension of E-O system performance to subpicosecond quantitative measurements.

References

[1] J.M. Wiesenfeld, "Electro-optic sampling of high-speed devices and integrated circuits," *IBM J. Res. Develop.,* vol.34, pp.141-161, 1990.

[2] S.Gupta, J.F.Whitaker, and G.A.Mourou, " Subpicosecond pulse propagation on coplanar waveguides: experiment and simulation," *IEEE Microwave and Guided Wave Letters,* vol.1, pp.161-163, 1991.

[3] Kurt J. Weingarten, Mark J. W. Rodwell and David M. Bloom, "Picosecond optical sampling of GaAs integrated circuits, " *IEEE J. of Quantum Electronics,* vol.24, pp.198-220, 1988.

[4] T.Nagatsuma, T.Shibata, E.Sano, and A.Iwata, "Subpicosecond sampling using a noncontact electro-optic probe," *J.Appl. Phys.,* vol.66, pp.4001-4009, 1989.

[5] Guo-Chun Liang, Yao-Wu Liu, and Kenneth K.Mei, "Full-wave analysis of coplanar waveguide and slotline using the time-domain finite-difference method, " *IEEE Trans. Microwave Theory Tech.,* vol.37, pp.1949-1957, 1989.

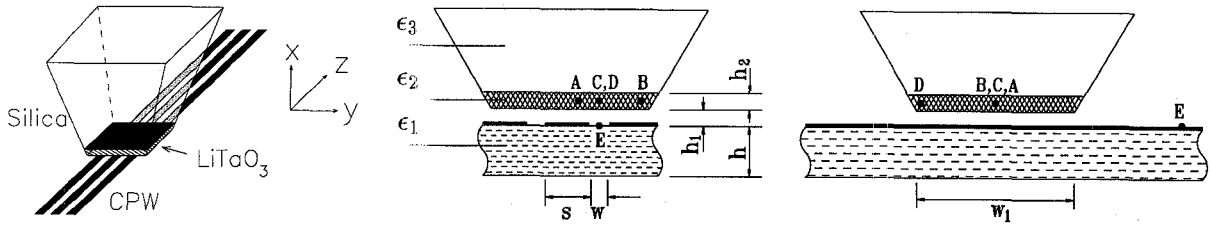

(a) (b) (c)

Figure 1: (a) Schematic of the coplanar waveguide(CPW) with the probe. The pulse propagates in z-direction. (b) Cross section of x-y plane. (c) Cross section of x-z plane.

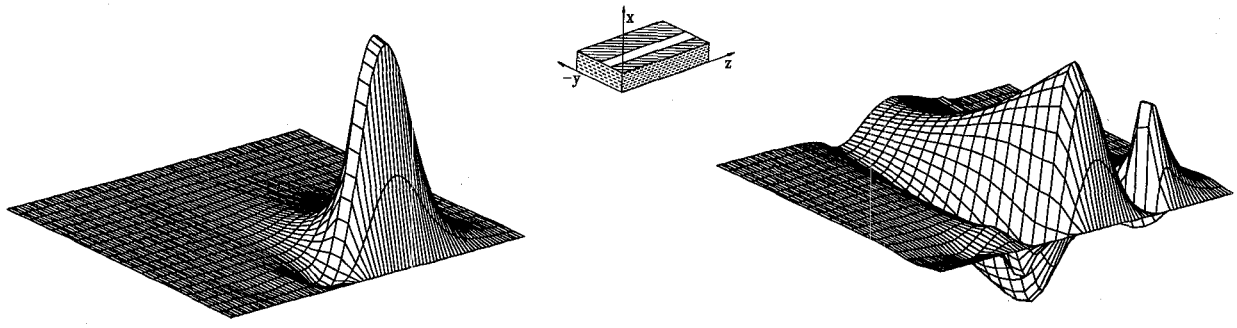

(a) (b)

Figure 2: The spatial waveforms of E_y $10\mu m$ above the CPW at $9ps$. The pulse propagates in z-direction. Only one side is shown in this figure due to the symmetry of the CPW field. (a) Without probe (Case 3). (b) With probe($h_1 = 10\mu m$ in Case 1).

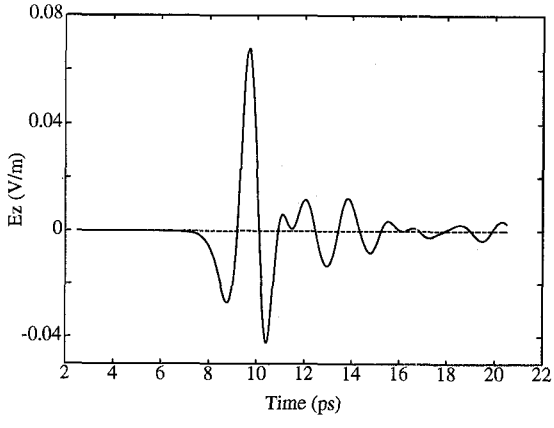

Figure 3: Comparison of E_z waveforms sampled at point C with probe($h_1 = 10\mu m$ in Case 1: solid line) and without probe (Case 3: dashed line). C is just above the center of CPW slot space. Z-axis is the CPW's longitudinal direction.

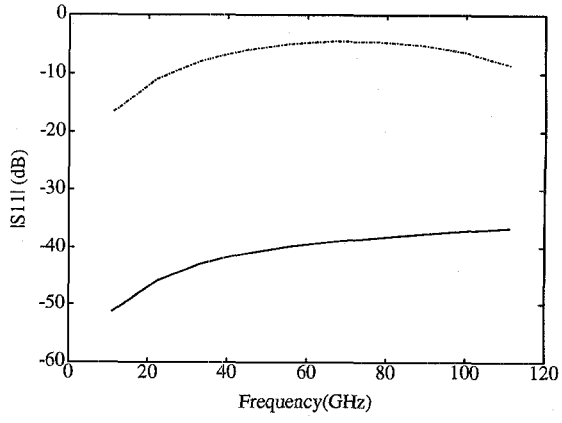

Figure 4: Magnitude of reflection coefficient $S_{11}(dB)$ of the CPW for Case 1($h_1 = 10\mu m$: solid line) and Case 2($h_1 = 0\mu m$: dashdot line).

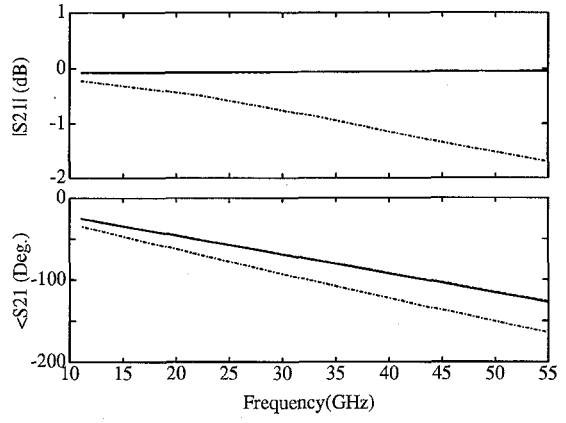

Figure 5: Transmission coefficient S_{21} of the CPW with probe for Case 1($h_1 = 10\mu m$: solid line), Case 2($h_1 = 0\mu m$: dashdot line) and without probe for Case 3(dashed line). Solid and dashed lines almost coincide with each other.

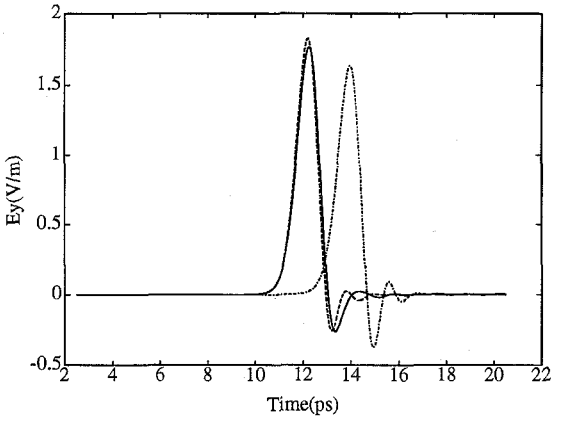

Figure 6: E_y waveforms sampled at the point **E** with probe for Case 1($h_1 = 10\mu m$: solid line), Case 2($h_1 = 0\mu m$: dashdot line) and without probe for Case 3(dashed line). Point **E** is after the probe with the distance of $364\mu m$ to point C.

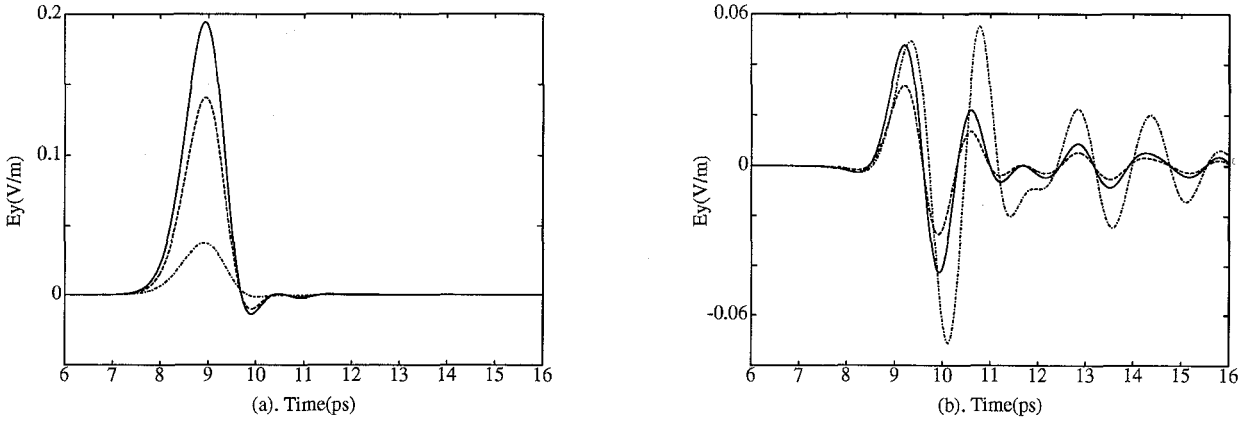

Figure 7: Comparisons of E_y waveforms at different points. (a). Without probe (Case 3). (b). With probe($h_1 = 10\mu m$ in Case 1). Sampled at point **C**: solid line. **C** is just above the center of CPW slot space. Sampled at point **A**: dashed lines. **A** is above the CPW center metal strip, $10\mu m$ away from **C**. Sampled at point **B**: dashdot line. **B** is above the CPW ground plane, $50\mu m$ away from **C**. (See Fig.1)

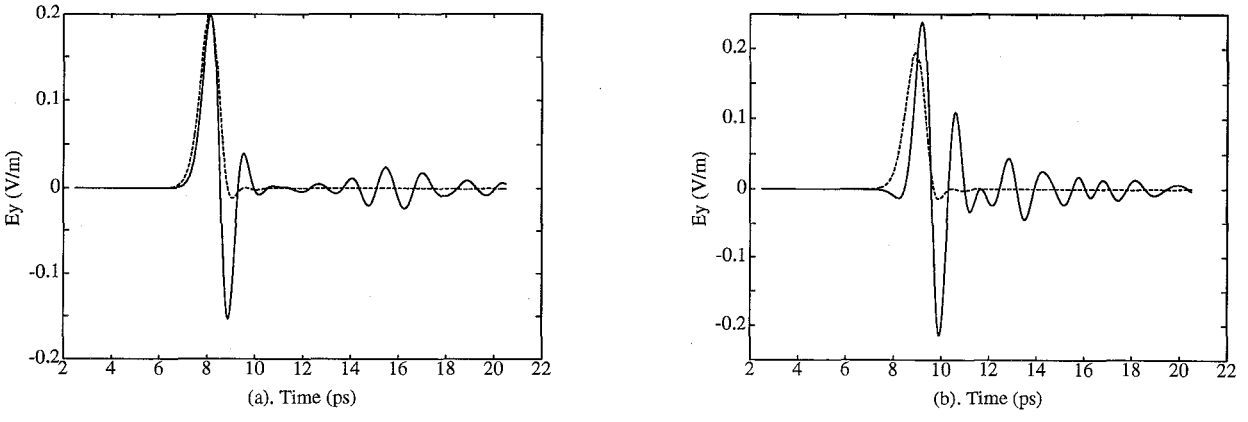

Figure 8: Comparisons of E_y waveform distortion with probe($h_1 = 10\mu m$ in Case 1: solid line) and without probe(Case 3: dashed line). (a). Sampled at **D**, $13\mu m$ away from the probe's edge. (b). Sampled at **C**, just above the center of CPW slot space. (Note plotted E_y for Case 1 is magnified by 5.0.)